Published in final edited form as:
Nature. 2014 October 23; 514(7523): 498–502. doi:10.1038/nature13814.

Dendritic Cells Control Fibroblastic Reticular Network Tension and Lymph Node Expansion

Sophie E. Acton[1,2], **Aaron J. Farrugia**[1,3], **Jillian L. Astarita**[4], **Diego Mourão-Sá**[1,*], **Robert P. Jenkins**[3], **Emma Nye**[5], **Steven Hooper**[3], **Janneke van Blijswijk**[1], **Neil C. Rogers**[1], **Kathryn J. Snelgrove**[1], **Ian Rosewell**[6], **Luis F. Moita**[7], **Gordon Stamp**[5], **Shannon J. Turley**[4], **Erik Sahai**[3], and **Caetano Reis e Sousa**[1]

[1]Immunobiology Laboratory, Cancer Research UK London Research Institute, 44 Lincoln's Inn Fields, London, WC2A 3LY, UK

[2]Department of Cell and Developmental Biology, University College London, Gower Street, WC1E 6BT, UK

[3]Tumour Cell Biology Laboratory, Cancer Research UK London Research Institute, 44 Lincoln's Inn Fields, London, WC2A 3LY, UK

[4]Department of Cancer Immunology and AIDS, Dana-Farber Cancer Institute, Boston, MA 02215, USA

[5]Experimental Histopathology Laboratory, Cancer Research UK London Research Institute, 44 Lincoln's Inn Fields, London, WC2A 3LY, UK

[6]Transgenics Laboratory, Cancer Research UK London Research Institute, Clare Hall Laboratories, South Mimms, Potters Bar, Hertfordshire, EN6 3LD, UK

[7]Instituto Gulbenkian de Ciência, Rua da Quinta Grande 6, 2780-156 Oeiras, Portugal and Instituto de Medicina Molecular, Faculdade de Medicina, Universidade de Lisboa, 1649-028 Lisboa, Portugal

Abstract

Following immunogenic challenge, infiltrating and dividing lymphocytes significantly increase lymph node (LN) cellularity leading to organ expansion[1,2]. Here we report that the physical elasticity of LNs is maintained in part by podoplanin (PDPN) signalling in stromal fibroblastic reticular cells (FRCs) and its modulation by CLEC-2 expressed on dendritic cells (DCs). We show that PDPN induces actomyosin contractility in FRCs via activation of RhoA/C and downstream Rho-kinase. Engagement by CLEC-2 causes PDPN clustering and rapidly uncouples PDPN from

Correspondence and requests for materials should be addressed to S.E.A. (sophie.acton@cancer.org.uk) or C.R.S. (caetano@cancer.org.uk).
*Current address: Laboratory of Immune Cell Epigenetics and Signaling, The Rockefeller University, 1230 York Avenue, New York, New York 10065, USA

Author Contributions: S.E.A, E.S. and C.R.S. designed the study, analysed data and wrote the manuscript. S.E.A. conducted experiments with assistance from A.J.F., J.v.B., R.P.J. K.J.S. and S.H. Preliminary results were generated with S.J.T. and J.L.A. E.N. and G.S. carried out immunohistochemistry and morphometric analysis. D.M.S., N.C.R and I.R. generated CD11c$^{\Delta CLEC\text{-}2}$ mice. N.C.R. managed breeding and genotyping of mouse strains. L.F.M. provided key reagents.

Europe PMC Funders Author Manuscripts

RhoA/C activation, relaxing the actomyosin cytoskeleton and permitting FRC stretching. Notably, administration of CLEC-2 protein to immunised mice augments LN expansion. In contrast, the latter is significantly constrained in mice selectively lacking CLEC-2 expression in DCs. Thus, the same DCs that initiate immunity by presenting antigens to T lymphocytes[3] also initiate remodeling of LNs by delivering CLEC-2 to FRCs. CLEC-2 modulation of PDPN signalling permits FRC network stretching and allows for the rapid LN expansion driven by lymphocyte influx and proliferation that is the critical hallmark of adaptive immunity.

LNs are meeting places for T lymphocytes and antigen presenting DCs[1,2]. T cell - DC interactions are supported by FRCs[4,5], a complex interconnected network that produces and ensheathes extracellular matrix components[6] that filter draining lymph[7]. FRC networks additionally provide physical routes for leucocyte traffic[1], and chemoattractants for T cells and DCs[5]. Additionally, contact with FRCs promotes chemokinesis in DCs facilitating their migration within LNs[8]. This is partly due to cytoskeletal changes in DCs induced upon signalling by the C-type lectin receptor CLEC-2 when it is engaged by PDPN expressed on FRCs[8]. Here, we asked whether, in addition to promoting DC movement along FRCs, CLEC-2 might also work in reverse, modulating PDPN function and altering the properties of the FRC network.

To examine PDPN signalling in fibroblasts, wild-type (WT) PDPN tagged with CFP (PDPN-CFP) was over-expressed in NIH/3T3 cells, which express only low levels of the endogenous protein[8]. Within 30h of transfection, CFP was detectable at the plasma membrane where it co-localised with Cherry-tagged ezrin, consistent with reports of a direct interaction between the two proteins[9,10] (Fig. 1a, Extended Data Video 1). Ezrin belongs to the family of closely related proteins, ezrin, radixin and moesin (ERM), which tether the actin cytoskeleton to the plasma membrane. We therefore examined localisation and phosphorylation of ERM proteins, along with myosin light chain (MLC), which mediates actin-dependent contraction, in PDPN-CFP overexpressing cells. In contrast to untransfected cells, PDPN-CFP^{+} NIH/3T3 cells displayed pERM and pMLC accumulation at the cell cortex (Fig. 1a) and often rounded up, features typical of contractile cells[11-14]. A non-phosphorylatable ezrin T567A mutant formally demonstrated the key role of ERM phosphorylation in PDPN-driven cell contraction (Fig. 1b).

To determine which pathways connected PDPN to cell contraction, a chemical screen was conducted, which revealed relaxation upon inhibition of RhoA/C, ROCK, or Myosin II (Extended data Fig. 1a, b). Strikingly, treatment with soluble recombinant CLEC-2-Fc protein phenocopied RhoA/C and ROCK inhibition, almost completely reversing the contraction induced by PDPN-CFP (Fig. 1c). The inhibition by CLEC-2 was rapid but transient (Fig. 1c) and led to ezrin re-distribution from the plasma membrane to the cytoplasm (Fig. 1d). To test this in FRCs expressing physiological levels of PDPN, we generated LN FRC lines (Extended Data Fig. 2 and Methods). Sub-lines stably expressing FRET biosensors reporting RhoA or Rac1 activity were exposed to CLEC-2-Fc-coated 10 μm beads. In agreement with the NIH/3T3 studies, RhoA activity was immediately and robustly reduced when CLEC-2-beads made contact with FRCs (Fig. 1e and Extended Data Video 2). Sudden loss of RhoA activity was also evident from temporary loss of adhesion[15]

(Extended Data Videos 2 and 3). In contrast, Rac1 activity gradually increased after exposure to CLEC-2 beads (Fig. 1e, and Extended Data Video 3), which was confirmed in longer-term experiments by pulldown of GTP-bound Rac1 (Fig 1f). Higher Rac1-GTP levels, increased ARP2/3$^+$ lamelipodial protrusions and tail retraction defects were also observed in FRCs when PDPN was stably depleted (PDPN KD FRCs; Fig. 1f and Extended data Fig. 3). To identify guanine-nucleotide exchange factors (GEFs) that may connect PDPN to activation of RhoA/C, we decreased expression of candidates using siRNA and found that PDPN-induced contractility primarily requires GEF-H1 in NIH/3T3 and FRCs (Extended data Fig. 1c, d). We also looked for further changes in FRCs consistent with decreased RhoA/C activity and found that PDPN knockdown or engagement by CLEC-2 caused rapid dissolution of stress fibres (Fig. 1g, Extended Data Video 4, Extended data Figs. 3, 4). Thus, PDPN in fibroblasts associates with ezrin and signals to promote RhoA/C-dependent actomyosin-driven contraction. This is alleviated by CLEC-2 engagement, causing uncoupling of PDPN from ezrin and a RhoA/C to Rac1 switch. We hypothesise that Rac1 activity is increased indirectly as a consequence of reduced RhoA/C activity[14,16].

The cytoplasmic tail of PDPN undergoes phosphorylation and ezrin recruitment requires basic residues surrounding serine 167 (S167) [10,17]. We therefore tested whether phosphorylation of S167 controlled PDPN-induced contractility. Over-expression of PDPN (S167A) mutant failed to cause contraction in NIH/3T3 fibroblasts and occasionally caused collapse of the cytoskeleton, potentially by inhibiting activity of low levels of endogenous PDPN (Fig. 2a). In contrast, a PDPN S167E phosphomimetic mutant induced contractility comparable to WT protein (Fig. 2a, b). Inhibition of ROCK blocked contraction by both WT and S167E PDPN (Fig. 2b), placing ROCK activity downstream of S167 phosphorylation. However, CLEC-2-Fc treatment, whilst inhibiting contraction induced by WT PDPN, had no effect on S167E PDPN (Fig. 2b), suggesting that regulation of the phosphorylation status of S167 is one mechanism by which CLEC-2 uncouples PDPN from actomyosin contractility.

We considered how FRCs express high levels of endogenous PDPN yet, unlike transfected NIH/3T3 cells, do not display hypercontractility. As PDPN remained at the plasma membrane when engaged with CLEC-2 (Fig. 1d), we hypothesised that it partitions between active and inactive pools, the latter being maintained by binding to an inhibitory partner such as CD44[18,19]. FRCs express high levels of both PDPN and CD44[4] and knockdown of PDPN led to a concordant reduction of CD44 (Fig. 2c), suggesting an interaction. NIH/3T3 express low levels of CD44, perhaps accounting for their susceptibility to contract following PDPN overexpression. Consistent with that notion, co-transfection of CD44 and PDPN into NIH/3T3 fibroblasts markedly inhibited contraction (Fig. 2d).

CD44 resides within cholesterol-rich lipid rafts[19] and we tested whether CLEC-2 induces PDPN redistribution to such rafts. In steady state FRCs, PDPN and lipid rafts were found in small, partial colocalised clusters (Fig. 2e), as described in epithelial cells[20]. CLEC-2-Fc treatment induced formation of larger clusters in which PDPN and lipid rafts were more often colocalised (Fig. 2e). Notably, depletion of cholesterol from FRC membranes with methyl-β-cyclodextrin (MβCD) increased contractility, which was prevented by PDPN knockdown (Fig. 2f). CLEC-2 no longer inhibited PDPN-induced contraction in NIH/3T3

pre-treated with MβCD (Fig. 2g). Together, these data support the notion that CLEC-2 sequesters PDPN within lipid rafts, where increased interaction with CD44 prevents signalling to RhoA/C. Interestingly, CD44 can itself also drive contractility when excluded from lipid rafts (data not shown) suggesting a mutually inhibitory interaction with PDPN.

To explore the biological significance of PDPN/CLEC-2 interactions for FRC function, we examined cell behaviour in 3D collagen gels. Notably, FRCs reorganised the gel matrix to occupy a smaller volume and this was inhibited by CLEC-2 treatment or PDPN knockdown (Fig. 3a). Furthermore, CLEC-2 treatment or PDPN knockdown caused marked elongation of FRCs in 3D culture (Fig. 3b, Extended data Fig. 5). To determine the relevance of FRC stretching for LN dynamics, we investigated FRC network changes following induction of inflammation in vivo, which leads to upregulation of CLEC-2 by both LN resident and migratory DCs[8,21]. We first examined the cellular composition of draining LNs after subcutaneous immunisation of mice with ovalbumin (OVA) in complete Freund's adjuvant (CFA). During the afferent phase (days 0-6), T and B cell numbers increased rapidly and total LN cellularity augmented 2-3 fold (Extended data Fig. 6). However, numbers of FRCs ($CD45^-$ $PDPN^+$ $CD31^-$) remained constant until day 6 (Fig. 3c). This lag in FRC proliferation has been previously observed[22] although the kinetics likely depend on the type and strength of the inflammatory stimulus. In contrast, blood endothelial cells (BECs; $CD45^-$ $PDPN^-$ $CD31^+$), a distinct LN stromal population, increased in number from the earliest timepoint (Extended data Fig. 6).

If FRCs do not proliferate during early stages of acute inflammation, then to accommodate increased LN size the FRC network needs to 'stretch' to avoid disruption[22]. Consistent with that, the mean forward scatter of LN FRCs, an indication of cell size, increased after immunisation (Fig. 3d)[22] despite no loss of integrity of the FRC network (Fig. 3e). A gap analysis algorithm[23] revealed significantly larger spaces between the reticular network branches after immunisation, consistent with FRC stretching (Fig. f). In a complementary approach, we utilised PDGRFaKI-H2B-GFP mice (Extended data Fig. 7) and calculated the spacing between FRC nuclei (GFP^+) using automated morphometric analysis software, which confirmed that FRCs spread further apart after immunisation (Fig. 3g). Together, these data indicate that FRCs expand and that the pre-existing FRC network enlarges in response to acute inflammation such as following immunisation.

The profound cytoskeletal changes in FRCs following CLEC-2 binding in vitro, suggested that inhibition of PDPN-induced contractility by CLEC-2^+ DCs might aid FRC network enlargement in vivo. Consistent with this, LN influx of immigrant DC ($CD45^+$, $CD11c^+$, $MHCII^{hi}$) bearing high CLEC-2 levels[8] peaked at day 2 post OVA/CFA immunisation (Fig. 3c). We therefore examined LN architecture and expansion in CD11cCre × $Clec1b^{loxP/loxP}$ mice ($CD11c^{\Delta CLEC\text{-}2}$). These mice display selective ablation of CLEC-2 in $CD11c^+$ cells (Extended data Fig. 8), the majority of which within the T cell zone are DCs. Interestingly, in >24 week old $CD11c^{\Delta CLEC\text{-}2}$ mice, steady state LN size was significantly reduced compared to controls (Fig 4a), which was not the case in younger mice (Fig. 4b; non-draining LN). However, following immunisation, expansion of draining LNs was attenuated and spaces within the FRC network were smaller in young $CD11c^{\Delta CLEC\text{-}2}$ mice compared to

controls (Fig. 4b, c). Finally, LNs of CD11c$^{\Delta CLEC\text{-}2}$ mice remained more rigid and less deformable than controls following immunisation (Fig 4d).

Attenuated expansion of LNs in CD11c$^{\Delta CLEC\text{-}2}$ mice could be due to reduced numbers of immigrating DCs, reducing antigen availability and limiting T cell expansion. However, similar results were obtained upon administration of incomplete Freund's adjuvant without OVA or mycobacterial antigens (data not shown). Moreover, treatment by subcutaneous injection of recombinant CLEC-2-Fc protein but not a control Fc reagent (data not shown) following CFA/OVA immunisation markedly augmented LN expansion (Fig. 4e) and, importantly, completely rescued defects in LN expansion in CD11c$^{\Delta CLEC\text{-}2}$ mice (Fig 4e). The latter result indicates that diminished CLEC-2 provision rather than a dearth of immigrant antigen-presenting DCs limits LN expansion in CD11c$^{\Delta CLEC\text{-}2}$ mice. In sum, these data suggest that CLEC-2 delivery by DCs is required for maintaining FRC network architecture in vivo and is permissive for acute increases in LN size driven by cell influx provoked by local inflammation.

LNs are dynamic structures that must rapidly expand to accommodate leucocyte recruitment and proliferation. Given that LNs can expand 10-fold during adaptive immune responses while maintaining integrity, stromal components must by necessity proliferate[22,24]. However, in early phases of adaptive immune responses or in response to acute inflammation, FRC proliferation is insufficient to account for lymph node expansion (Fig. 3b and [22]). Here, we show that early LN expansion is permitted by FRC network relaxation, induced by increased availability of CLEC-2^{hi} DCs. We previously reported that CLEC-2 engagement by PDPN promotes DC migration along the FRC network[8]. Our data now show that PDPN is not simply a ligand for CLEC-2 but that it also reverse signals into FRCs to control actomyosin contractility. Our results suggest that a function of endogenous PDPN on FRCs is to cause stromal network contraction and create physical tension in LNs. This is offset by constant contact between FRCs and CLEC2^{+} resident DCs, balancing contractility and controling LN cellularity. The influx of additional CLEC-2^{hi} DCs, combined with the upregulation of CLEC-2 on resident DCs during acute inflammation[8], increases inhibition of PDPN, allowing the FRC network to stretch. We predict that this same mechanism can promote LN reduction as the short wave of increased CLEC-2 availability ends and PDPN activity returns. Whether the underlying collagen network is similarly elastic and to what extent acts to limit or promote LN expansion is as-yet unaddressed. Interestingly, CLEC-2 is not sufficient for LN expansion as administration of CLEC-2-Fc in the absence of inflammation did not affect LN size. Rather, CLEC-2 inhibition of PDPN is permissive for stretching and the influx of leucocytes via the HEV and afferent lymph likely provides the force for expansion. It is interesting to speculate that the stretching mechanism described in this study may also help initiate subsequent FRC proliferation given the emerging connections between tension and cell cycle regulation[25].

Methods

Mice

Experiments were performed in accordance with national and institutional guidelines for animal care and approved by the Institutional Animal Ethics Committee Review Board,

Cancer Research UK and the UK Home Office. Wild-type C57BL/6J mice were purchased from Charles River Laboratories (Wilmington, MA). PDGFRaKI-H2B-GFP mice (B6.129S4-*Pdgfratm11(EGFP)Sor*/J) were purchased from Jackson laboratories. To generate Clec1b floxed mice on a C57BL/6 background, C57BL/6 mouse clec1b genomic regions were cloned into a pFloxRI+TK targeting vector from the BAC clone R248K14 using the Red/Et recombination of Quick and Easy BAC modification kit (Gene Bridges, Dresden – Germany). Primers used were:

Clec1b BAC Fwd

TATTACCTGATGCTGTTACATCTCAGCTCTGCAGTATTTAGCCACCTTAGAGTTCCTAGCTGCTGACTCTgggtaccgagctcgaattctaccg

Clec1b BAC Rev

(CTGGGTTCTTTCCAGCTTCTGGCTATTATAAATAAGGCTGTTATGAACATAGTGGAGCATGTGTCCTTCTTgcggccgccaccgcggtggagctcca)

Upper case represent regions homologous to clec1b regions and lower case represent regions homologous to pFloxRI+TK vector. PCR was performed using Pwo DNA polymerase (Roche) following the manufacturer's instructions.

The 5′ loxP site was introduced in the intronic region between exon 1 and exon 2 by insertion of the loxP-pgk-gb2-NEO-loxP cassette (Gene Bridges, Dresden – Germany) using the following primers:

1st loxP Fw

AAAACCCAAAACCAAAAAACCAAAACCAACAACAAAACAAAAAAACAGATaattaaccctcactaaagggcg

1st loxP Rv

ACTTATTCTCTGTCCATTCTAACATATAACTGGCTACCAAGGCCACGTGTtaatacgactcactatagggctc

Upper case represent regions homologous to clec1b regions and lower case represent regions homologous to loxP-pgk-gb2-NEO-loxP cassette. PCR was performed using Pwo DNA polymerase (Roche) following the manufacturer's instructions.

The vector was then transformed into CRE-expressing *E. coli* EL350 (kind gift from Axel Behrens) leading to recombination of the cassette and leaving a single loxP site.

Next, the FRT-pgk-gb2-NEO-FRT-loxP cassette was introduced into the intronic region between exon 4 and exon 5 using the following primers:

Fw Rb2

tcccatgtcaagcattttggaatgctgaggggaaacattgaaatgctgttaattaaccctcactaaagggc

Rv Rb2

tctcagaggagcacacagtgcaaaccattaagaaacacatgaaaaggaaataatacgactcactatagggctcg

Upper case represent regions homologous to clec1b regions and lower case represent regions homologous to FRT-pgk-gb2-NEO-FRT-loxP cassette. PCR was performed using Pwo DNA polymerase (Roche) following the manufacturer's instructions.

The targeting vector was linearised by SfiI digestion (New England Biolabs), precipitated by phenol/chloroform and electroporated into PRX-B6N C57BL/6N embryonic stem (ES) cells.

Screening for homologous recombination in ES and mice was done by PCR using primers inside the FRT-pgk-gb2-NEO-FRT-loxP and outside the homology arm:

C1b Gen Rv – agaccctgagaaggctgga

NEO 3′ sense – gctcccgattcgcagcgcatc

Deletion of the NEO cassette was performed by crossing Clec1b-targeted mice with βActin-Flp (B6.Cg-Tg(ACTFLPe)9205Dym), and thereafter generating Clec1b$^{lox/lox}$ by interbreeding and screening for deletion of the NEO cassette using the following primers:

Seq FRT Fw (cctggtaaggagggtcccat) and Seq FRT Rv (atgagtctgctagggatgct).

Generation of CD11cΔCLEC-2 was achieved by crossing Clec1b$^{lox/lox}$ with CD11c-Cre mice (B6.Cg-Tg(Itgax-cre)1.1Reiz; kind gift from Boris Reizis). Both males and females were used for in vivo experiments and were aged 8-12 weeks unless otherwise stated in figures. Cre negative littermates were used as controls in all experiments.

qPCR analysis of Clec1b mRNA

CD11c+ cells from day 9 cultures of bone marrow in GM-CSF (BMDC) and treated with LPS for 6h or from spleens were enriched by MACS using CD11c beads (Miltenyi). RNA was extracted using an RNeasy mini kit (Qiagen) and cDNA generated using Superscript II reverse transcriptase (Invitrogen). qPCR was carried out using Sybr Green comparing Clec1b expression to GAPDH in each sample. Primers for Clec1b: Forward – TTTGAGCACAAGTGCAGCCCC, Reverse – AAGCAGTTGGTCCACTCTTG.

Constructs

PDPN-CFP was as previously described[8]. RhoA and Rac-1 FRET biosensors were kindly provided by Michiyuki Matsuda. GFP-MLC was as previously described[12]. PDPN WT and mutants S167A and S167E were cloned into pcDNA3.1-V5-His by PCR using EcoR1 and Not-1 restriction sites.

Cell lines

NIH/3T3 fibroblasts were cultured in Dulbecco's modified Eagle's medium (DMEM) + glucose (Life Technologies, Invitrogen, CA, USA) with 10% fetal bovine serum (FBS) and penicillin and streptomycin (PS). Cells were incubated and maintained at 37°C in 5% CO_2.

Mouse LN FRC lines were generated by first digesting skin-draining lymph nodes from C57BL/6 mice and then culturing adherent stromal cells as previously reported[8]. On day 4, stromal cells were immortalised by infection with HPV-E6-encoding retrovirus and selected with 2.5 μM puromycin as for the generation of carcinoma-associated fibroblast cell lines[26]. Immortalised FRCs were isolated by sequential MACS depletion of $CD45^+$ and $CD31^+$ cells using biotin conjugated antibodies and anti-biotin beads (Mitenyi). FRC cell lines and maintained in DMEM + glucose (Life Technologies, Invitrogen, CA, USA) with 10% FBS, penicillin/streptomycin and 1% Insulin-Transferrin-Selenium (Life Technologies, Invitrogen, CA, USA) at 37°C in 5% CO_2, and split using cell dissociation buffer (Life Technologies, Invitrogen, CA, USA). Stable knockdown of PDPN in FRCs was achieved with 2 different shRNA lentiviruses obtained from The RNAi Consortium of the Broad Institute (Cambridge, USA) that targeted the following sequences: GCTGCATCTTTCTGGATAATA (PDPN KD1) and GTTCTCCCAACACATCTGAAA (PDPN KD2). FRC cell lines expressing RhoA or Rac1 biosensors were generated by cotransfection of the biosensor plasmid with PiggyBac transferase using lipofectamine 2000, followed by selection with 5 μM blasticidin for 2 weeks. GFP-MLC expressing FRC cell lines were generated by lentiviral transduction and cell sorting. All cell lines were regularly tested for absence of mycoplasma contamination by the Cell Services Laboratory, Cancer Research UK London Research institute.

Over-expression studies

NIH/3T3 cells were plated at a density of 50,000 cells/ml in a glass-bottomed 24 well plate (MatTek, MA, USA) the day before transfection with plasmids encoding GFP, PDPN-CFP or PDPN-V5-his using Effectene transfection reagent (Qiagen, Hilden, Germany) as per supplier's instructions. After 24 hours, cells were treated with chemical inhibitors at the concentrations indicated (see Extended data Fig. 1b) for 6 hours before fixation. CLEC-2-Fc was added at 10 μg/ml for the time indicated in figures before fixation. In cotransfection experiments, plasmids encoding PDPN-CFP and ezrin-Cherry or PDPN-V5-his and CD44-GFP were added in equal amounts to the transfection mix. The cells were analysed by fluorescence microscope (20×, Nikon Eclipse Te2000-S, Tokyo, Japan) and contraction status scored manually. Cells were grouped into either contracted, partially contracted, spread or collapsed, depending on their morphology. High-resolution images were taken using a confocal microscope (Zeiss 710 using a 20×/0.8NA objective).

Immunofluorescence staining

Cells were fixed with 4% paraformaldehyde (PFA) in PBS for 10 minutes before permeabilisation in PBS containing 0.2% Triton-X for 10 minutes at room temperature. The cells were stained with DAPI (Sigma, d9542, MO, USA) to reveal DNA in cell nuclei and TRITC-phalloidin (Sigma, p1951, MO, USA) to reveal F-actin in 3% bovine serum albumin with PBS + 0.1% Tween-20. Cells were stained using anti-pMLC (S19) (Cell signaling technology #3675) or anti-pERM antibody (Cell signaling technology #3141) followed by appropriate Alexafluor-conjugated secondary antibodies (Invitrogen). PDPN-V5 was stained using anti-V5 FITC-conjugated antibody (Invitrogen R963-25). ARP2/3 was stained using Anti-p34-Arc/ARPC2 antibody (07–227 Millipore).

Lipid raft colocalisation analysis

Lipid raft labelling was carried out on ice on unfixed cells according to manufacturer's instructions (Vybrant lipid raft labelling kit 555, Invitrogen). Cells were then fixed in 4% paraformaldehyde before staining for PDPN (8.1.1 AF660-conjugated (eBioscience 50-5381-80). Confocal immunofluorescence images (63×/1.4NA oil immersion objective) of FRCs plated on glass either untreated or treated with 10 μg/ml CLEC-2-Fc for 30 minutes prior to staining were analysed using Zen image analysis software (Zeiss). Correlation coefficient R was calculated based on pixel intensity.

CLEC-2-Fc treatment in vitro

Generation of CLEC-2-Fc was as previously described[8]. Soluble CLEC-2 was used at 10 μg/ml diluted in cell culture medium. For CLEC-2-beads, 10 μm protein A-coated microspheres (Bangs laboratories) were incubated with 100 μg/ml CLEC-2-Fc diluted in PBS for 1 hour at 4°C then washed with cell culture medium. CLEC-2-Fc or CLEC-2-beads were added for the time indicated in the figures before fixation.

Lymph node expansion in vivo

Mice were immunised with 100 μl of an emulsion of OVA in CFA (100 μg OVA per mouse) or PBS in IFA subcutaneously in the right flank. Draining inguinal lymph nodes were taken for analysis at the indicated days post-immunisation; left-side non-draining lymph nodes were taken for comparison. Where mice were treated with CLEC-2-Fc, they received 10 μl (1 μg in PBS) subcutaneously adjacent to site of immunisation on days 1 and 3. Lymph nodes were first weighed, then digested as previously described[27]. Cells were counted and stained for flow cytometry analysis. Alternatively, intact lymph nodes were fixed in 10% formalin for immunohistochemistry analysis.

Lymph node deformation assay

Draining and non-draining inguinal lymph nodes were taken from $CD11c^{\Delta CLEC\text{-}2}$ mice and littermate controls on day 5 following CFA immunisation. Lymph nodes were placed on the contact points of a digimatic thickness gauge (Mitutoyo, USA) and subjected to 1.4N of applied force. Deformability was calculated as follows: Deformability = 1 – (LN size under 1.4N/LN size before force was applied). Each LN was measured twice and the results averaged.

Flow cytometry

Cells isolated from LNs, FRCs or NIH/3T3 cell lines were suspended in FACS buffer (PBS 2% FCS, 2mM EDTA) and first blocked with anti-CD16/CD32 (eBioscience) for all staining procedures. Cells were counted on a FACS Calibur by reference to fluorescence beads. Stained cells were analysed on either a FACS Calibur or LSRII. Antibodies used for staining: CD45.1 (BD Biosciences), CD140a (clone APA5 eBioscience), CD31 (BD Biosciences), PDPN (clone 8.1.1 eBioscience), CD35 (clone 8C12 BD Biosciences), VCAM-1 (clone M/K-2 Abcam), CD44 (clone IM7 BD Biosciences), CD3 (BD Biosciences), CD19 (clone ID3 BD Biosciences), MHCII (I-A/I-E BD Biosciences), CD11c (clone HL3 BD Biosciences).

Europe PMC Funders Author Manuscripts

Immunohistochemistry

Tissue sections 4 μm thick were cut at 3 levels (with 150μm between the levels) from formalin-fixed paraffin-embedded lymph nodes. These sections were then stained using the Vector ABC elite detection system (PK6100 1:250,Vector laboratories, UK). Slides were first incubated with a primary antibody for 1 hour (anti-GFP: AB6673 1:350, Abcam, anti-PDPN: DM3501, Acris), followed by incubation with biotinylated-labelled secondary antibody (1:250, Vector laboratories, UK) for 45 min. ABC complex was then applied for 30 minutes and staining was completed by 3 min incubation with DAB and chromogen (SK 4100 Vector laboratories, UK). Slides were counterstained with hematoxylin and mounted. ER-TR7 staining was conducted on 10 μm thick frozen LN sections (Santa Cruz sc-73355-AF488)

Gap analysis

Quantification of gap sizes was carried out in MATLAB. PDPN signal was isolated and converted to grayscale. The images were thresholded, background subtracted, small objects removed, then converted to binary images using ImageJ software. A circle-fitting algorithm was applied whereby, in each step, the largest circle that could fit in the gaps and that did not overlap with other fitted circles was recorded. The distribution of radii of circles that fill the image was then weighted according to area such that larger circles had a proportionally greater weighting than smaller circles. The plot of distribution of radii was smoothed to transform the data from a discrete pixel size distribution to a continuous micron size distribution. Raw data were analysed using Fisher's exact test ($p = 4.194e-09$) to determine differences in circles with radius >15 μm. Each analysis was performed on images of the FRC network from >8 individual mice per group. No images were excluded from the analysis and all data were combined and are represented in the graphs shown (16 images per group). MATLAB script is available upon request.

Automated Morphometric analysis

The slides were digitised with a commercial image analysis system (Ariol; Leica Biosystems). The program was trained to recognise GFP+ stained nuclei by size, shape and staining intensity. T cell areas were identified by density of hematoxylin staining and traced out manually on each lymph node in the scan. Automated analysis then counted the total number of GFP+ nuclei in each T cell area, (24 areas analysed per group). Area/FRC nuclei were compared using Mann Whitney U test.

Rac1GTP pulldown assay

FRC cell lines either treated with CLEC-2-Fc for 30 minutes or stably depleted of PDPN (shRNA) were subjected to Rac1 pulldown and analysis as per manufacturer's instructions (kit 16118 Pierce). Rac-1 levels in pulldowns and whole lysate were compared by Western blot.

3D cell culture and gel contraction assay

Control or PDPN KD FRCs were seeded at 10,000 per well in 150 μl collagen/matrigel matrix[8,26,28]. Gels were set at 37°C for 30 minutes then covered with cell culture medium.

In some wells, the following were added to both the gel mix and medium: 10 μg/ml CLEC-2-Fc, 10 μM ROCK inhibitor (Y27632) or 10 μg/ml anti-PDPN antibody (R&D, AF3244). Contraction of the gel at day 3 was quantified as the ratio of contracted gel/original area and plotted relative to control. Gels were stained with TRITC-labelled phalloidin and DAPI for maximum length analysis (Imaris). The furthest points of each individual cell were measured in x,y,z coordinates and vectors calculated for comparison (Extended data figure 5).

Statistics

Sample size for in vivo experiments was determined by litter size as littermate controls were used in all comparisons. For in vitro experiments, all cells within the sample were scored and none excluded and experiments were repeated at least once to ensure reproducibility and adequate statistical power. Category data from over-expression studies was analysed using Fisher's exact test (R software). Changes to contraction and morphology were analysed using Mann Whitney-U tests. Analysis of cell populations during a time course of immunisation was conducted with one-way ANOVA and followed by Kruskall-Wallis multiple comparisons test. Comparison of LN size and cellularity between control and $CD11c^{\Delta CLEC\text{-}2}$ across different treatment groups was analysed using 2-way ANOVA followed by multiple comparisons test between treatments and genotypes. Appropriate statistical tests were chosen for the data set following advice from a mathematician (R.P.J.). Chemical screen for cell contraction inhibitors was scored by an independent observer (A.F.) who was unbiased as to the predicted results.

Europe PMC Funders Author Manuscripts

Europe PMC Funders Author Manuscripts

Extended Data

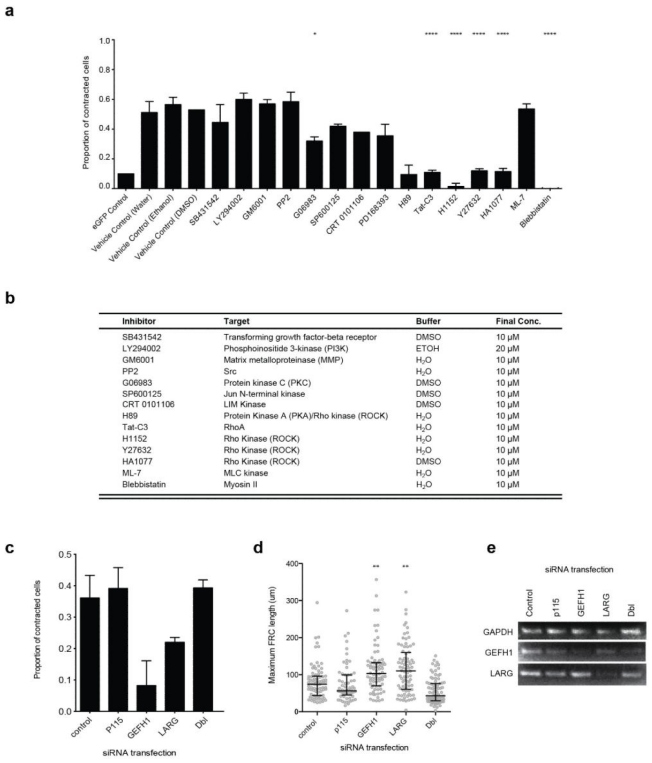

Inhibitor	Target	Buffer	Final Conc.
SB431542	Transforming growth factor-beta receptor	DMSO	10 μM
LY294002	Phosphoinositide 3-kinase (PI3K)	ETOH	20 μM
GM6001	Matrix metalloproteinase (MMP)	H_2O	10 μM
PP2	Src	H_2O	10 μM
G06983	Protein kinase C (PKC)	DMSO	10 μM
SP600125	Jun N-terminal kinase	DMSO	10 μM
CRT 0101106	LIM Kinase	DMSO	10 μM
H89	Protein Kinase A (PKA)/Rho kinase (ROCK)	H_2O	10 μM
Tat-C3	RhoA	H_2O	10 μM
H1152	Rho Kinase (ROCK)	H_2O	10 μM
Y27632	Rho Kinase (ROCK)	H_2O	10 μM
HA1077	Rho Kinase (ROCK)	DMSO	10 μM
ML-7	MLC kinase	H_2O	10 μM
Blebbistatin	Myosin II	H_2O	10 μM

Extended data Figure 1. Screen for inhibitors of PDPN-mediated cell contractility

a) Quantification of proportion of contracted NIH/3T3 fibroblasts expressing eGFP control or PDPN-CFP and treated with the indicated inhibitors or vehicles. Statistically significant inhibition: **** p <0.00001 and * p = 0.01, Fisher's Exact test. Data represent mean ± SD of 3 independent experiments. **b)** Chemical inhibitors used in (a) and their targets. **c)** Contraction score of PDPN-expressing NIH/3T3 fibroblasts transfected with siRNA smartpools targetting the indicated Rho GEFs (MU-046870-01-0002, MU-040120-00-0002, MU-047092-01-0002, MU-041056-01-0002, Dharmacon, GE Healthcare). **, p<0.05, one-way ANOVA. **d)** Maximum length of FRCs in collagen gels measured in 3-dimensions from 100 μm deep confocal z-stacks. Each point represents one FRC. **, p<0.05, one-way ANOVA. **e)** PCR analysis of RhoGEF mRNA expression in FRC cell lines following siRNA knockdown in comparison to expression of GAPDH.

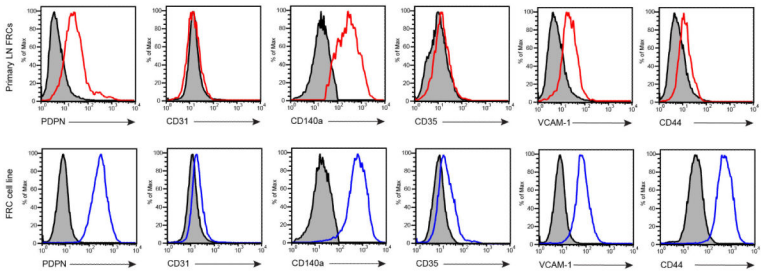

Extended data Figure 2. Generation of FRC lines

Europe PMC Funders Author Manuscripts

Comparison of an FRC cell line generated by immortalisation of primary FRCs (bottom panels, blue) with primary FRCs in LN cell suspensions cultured for 7 days (top panels, red). Gray histograms indicate isotype-matched control antibody staining. Histograms of primary LN cultures are gated on $CD45^{-}$ $CD140a^{+}$ cells to exclude haematopoietic cells and other stromal subsets. Histograms of the FRC cell line are gated only on live cells.

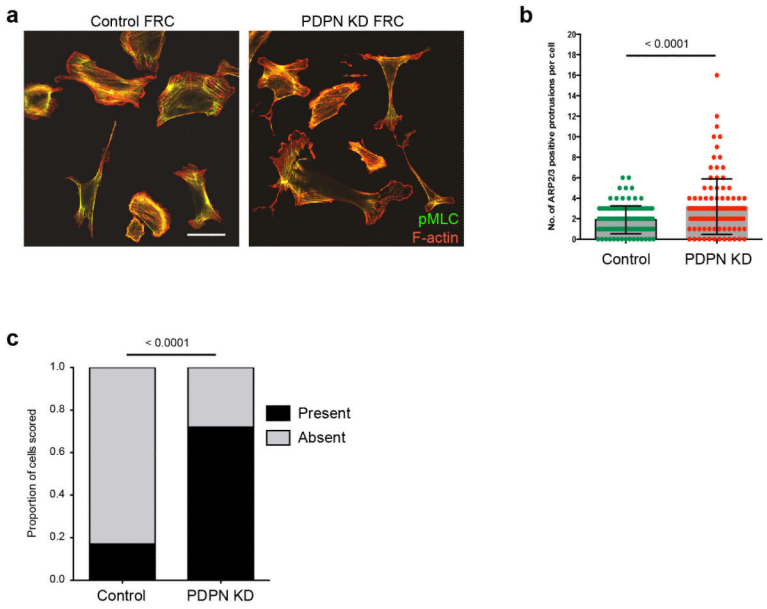

Extended data Figure 3. Loss of PDPN results in FRC spreading and actin polymerisation

a) Single optical slice (1 μm) showing morphology and pMLC organisation of control and PDPN KD FRCs. pMLC S(19) (green), F-actin (red). Scale bar indicates 50 μm **b)** Quantification of the number of ARP2/3 positive protrusions per FRC comparing control (green) and PDPN KD (red) cell lines. Data represent mean +/−SD, each point represents an individual FRC. $p<0.0001$ calculated using Mann Whitney U test. **c)** Quantification of tail retraction defects comparing control and PDPN KD FRCs. Data are collated from >100 cells, $p<0.0001$ calculated using Fisher's exact test. "Present" means that tail retraction defects were deemed present by the observer.

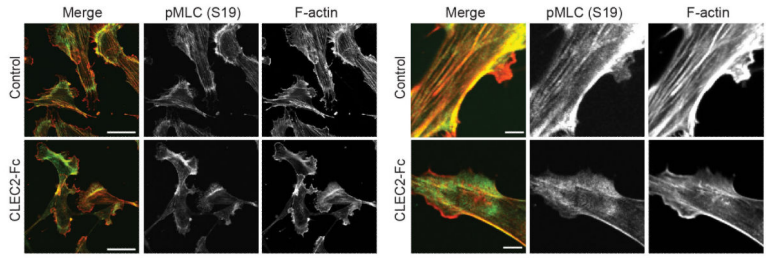

Extended data Figure 4. Loss of pMLC and F-actin filaments following treatment of FRCs with CLEC-2

Single optical slices (1 μm) of FRC cell lines treated for 30 min with 10 μg/ml soluble CLEC-2-Fc protein, fixed and stained for pMLC (S19) (green) and F-actin (red). Scale bar

represents 50 μm. Higher magnification shown in right hand panels. Scale bar represents 5 μm.

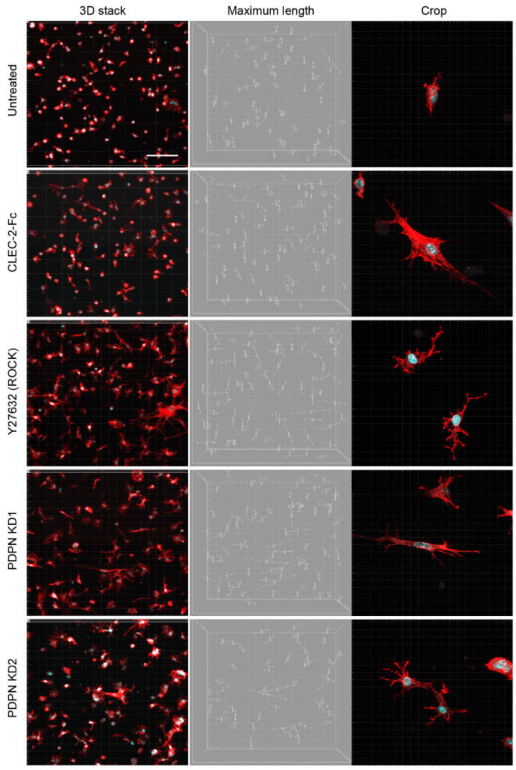

Extended data Figure 5. Elongated morphology of CLEC-2-treated FRCs in 3D cultures

Quantification of maximum cell length for 100 μm deep z-stacks. FRCs cultured in 3D collagen/matrigel matrix for 3 days treated with CLEC-2-Fc, ROCK inhibitor 10 μM (Y27632), or stably knocked down for PDPN expression. Left panel shows projection of the 3D stack; staining F-actin (red), DNA (cell nuclei, blue). Scale bar indicates 200 μm. Centre panel shows x,y,z coordinates and length of each vector for each end of each cell in 3D as quantified using Imaris image analysis software. Right panel shows example of cell morphology in each treatment group; staining F-actin (red), DNA (cell nuclei, blue). Scale bar indicates 50 μm.

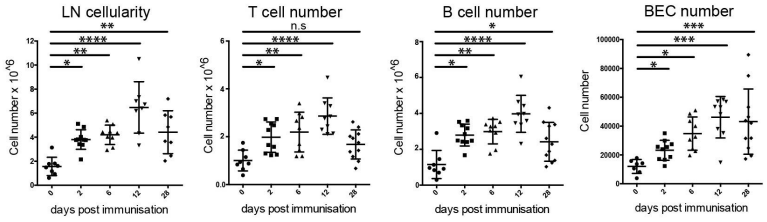

Extended data Figure 6. Timecourse of LN expansion following OVA/CFA immunisation

Total cellularity, number of T cells ($CD45^+$, $CD3^+$), B cells ($CD45^+$, $CD19^+$) and BEC ($CD45^-$ $PDPN^-$ $CD31^+$) in draining LNs at different times after OVA/CFA immunisation. Each point represents one lymph node and data show mean ± SD of 2 independent

Europe PMC Funders Author Manuscripts

experiments scoring 8-12 mice. Day 0 represents LNs from non-immunised mice. Asterisks represent statistically significant differences between non-immunised and immunised mice as calculated using 1-way ANOVA test followed by Tukey's multiple comparisons test (*, $p<0.05$, **, $p>0.001$, ***, $p>0.0001$, ****, $p<0.00001$).

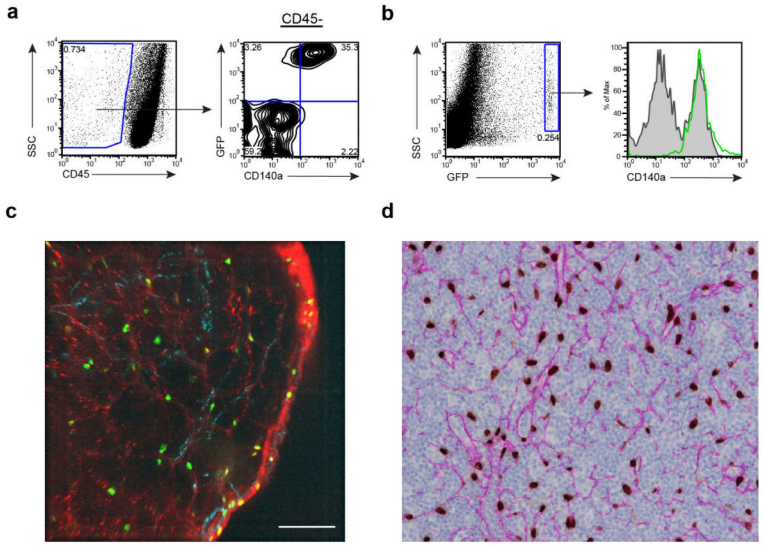

Extended data Figure 7. FRCs are selectively labelled in PDGFRαKI H2B-GFP mice

a) Analysis of skin draining LNs from PDGFRαKI H2B-GFP mice showing lymph node stromal cells co-expressing CD140a (PDGFRa) and GFP. Left panel shows gate for $CD45^-$ stroma, right panel shows GFP and CD140a expression of $CD45^-$ gate. **b)** Flow cytometry analysis showing that GFP^+ cells are $CD140a^+$. Left panel shows gating for GFP^+ LN cells, right panel shows CD140a expression of GFP^+ gate (green) compared to $CD45^-$ cells (gray) **c)** Z-stack of PDGFRαKI H2B-GFP lymph node imaged ex vivo using 2-photon microscopy. FRC nuclei (green), second harmonic signal (collagen) (blue). Wheat germ agglutinin AF647 (red) was injected subcutaneously 5 minutes prior to LN extraction to label conduits. Scale bar indicates 200 μm. **d)** Immunohistochemical staining of paraffin embedded sections of LNs from PDGFRαKI H2B-GFP mice. Staining GFP (brown) and PDPN (pink), counterstained with haematoxylin (blue).

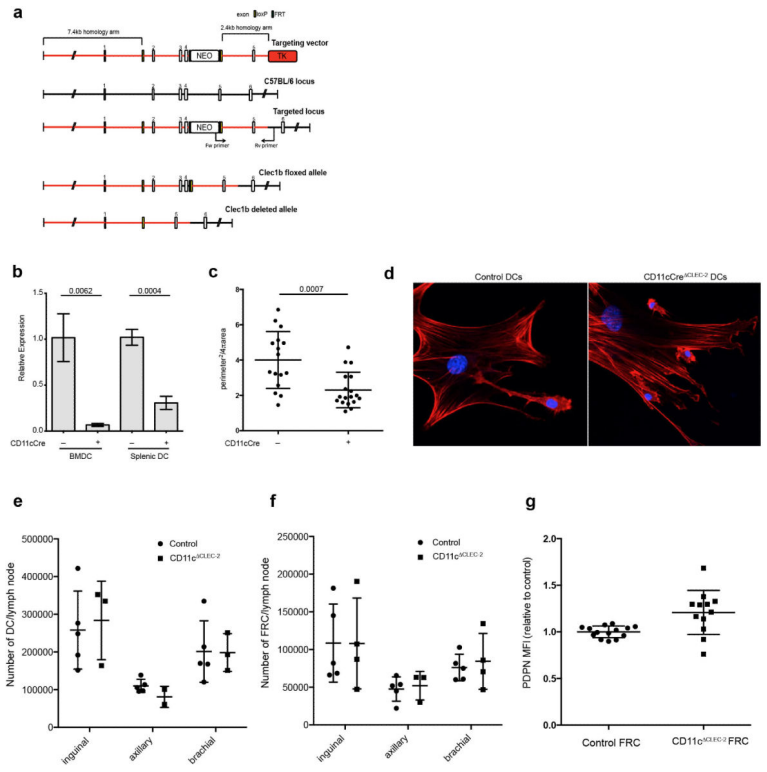

Extended data Figure 8. Generation and characterisation of CD11c$^{\Delta CLEC\text{-}2}$ mice

a) Scheme of targeting approach to allow conditional deletion of Clec1b exons 2,3, and 4. loxP sites shown in yellow. **b)** Clec1b mRNA in LPS-treated BMDC or freshly isolated CD11c^{+} splenocytes from CD11c$^{\Delta CLEC\text{-}2}$ mice and Cre^{neg} littermates. Data are represented as relative expression compared to control and depict mean ± SD from 6 replicates from 2 independent experiments. p values calculated using Students's t test. **c)** Quantification of bone marrow derived DC morphology cultured in contact with FRCs. Data indicate score of perimeter^{2}/4πarea, area and perimeter calculated from immunofluorescence imaging using ImageJ software. Higher scores indicate increased elongation and/or protrusions. p=0.0007 calculated using Mann Whitney U test. **d)** Representative images from (c) showing DCs spreading over FRCs. F-actin (red), cell nuclei (blue). **e)** Total DC numbers and **f)** total FRC numbers in steady state skin-draining LNs of control vs CD11c$^{\Delta CLEC\text{-}2}$ mice. Each data point represents one lymph node. **g)** PDPN surface expression by FRC from control and CD11c$^{\Delta CLEC\text{-}2}$ mice as measured by flow cytometry and represented relative to the control group. MFI, mean fluorescence intensity.

Extended Data Videos

Refer to Web version on PubMed Central for supplementary material.

Acknowledgements

We thank Boris Reizis for CD11c-Cre mice, the LRI Biological Resources staff for animal care and assistance with experiments and Rachel Horton-Harpin at LRI Cell Services for production of CLEC-2-Fc. We are grateful to Michael Y. Gerner and Ronald N. Germain for critical reading of the manuscript and all members of the Immunobiology laboratory and Tumour Cell Biology Laboratory for helpful discussions and comments. This work

Europe PMC Funders Author Manuscripts

was supported by a Henry Wellcome Postdoctoral fellowship (SEA) and core funding from Cancer Research UK (IR, GS, ES and CRS).

References

1. Girard J-P, Moussion C, Förster R. HEVs, lymphatics and homeostatic immune cell trafficking in lymph nodes. Nat Rev Immunol. 2012; 12:762–773. [PubMed: 23018291]
2. Junt T, Scandella E, Ludewig B. Form follows function: lymphoid tissue microarchitecture in antimicrobial immune defence. Nat Rev Immunol. 2008; 8:764–775.
3. Banchereau J, Steinman RM. Dendritic cells and the control of immunity. Nature. 1998; 392:245–252.
4. Link A, et al. Fibroblastic reticular cells in lymph nodes regulate the homeostasis of naive T cells. Nat. Immunol. 2007; 8:1255–1265. [PubMed: 17893676]
5. Katakai T. A novel reticular stromal structure in lymph node cortex: an immuno-platform for interactions among dendritic cells, T cells and B cells. International Immunology. 2004; 16:1133–1142. [PubMed: 15237106]
6. Sixt M, et al. The Conduit System Transports Soluble Antigens from the Afferent Lymph to Resident Dendritic Cells in the T Cell Area of the Lymph Node. Immunity. 2005; 22:19–29. [PubMed: 15664156]
7. Gretz JE, Anderson AO, Shaw S. Cords, channels, corridors and conduits: critical architectural elements facilitating cell interactions in the lymph node cortex. Immunological reviews. 1997; 156:11–24.
8. Acton SE, et al. Podoplanin-Rich Stromal Networks Induce Dendritic Cell Motility via Activation of the C-type Lectin Receptor CLEC-2. Immunity. 2012; 37:276–289.
9. Ivetic A, Ridley AJ. Ezrin/radixin/moesin proteins and Rho GTPase signalling in leucocytes. Immunology. 2004; 112:165–176.
10. Martin-Villar E, et al. Podoplanin binds ERM proteins to activate RhoA and promote epithelial-mesenchymal transition. Journal of Cell Science. 2006; 119:4541–4553. [PubMed: 17046996]
11. Olson MF, Sahai E. The actin cytoskeleton in cancer cell motility. Clinical and experimental metastasis. 2009; 26:273–287. [PubMed: 18498004]
12. Wyckoff JB, Pinner SE, Gschmeissner S, Condeelis JS, Sahai E. ROCK- and myosin-dependent matrix deformation enables protease-independent tumor-cell invasion in vivo. Curr. Biol. 2006; 16:1515–1523. [PubMed: 16890527]
13. Lee J-W, et al. Peripheral antigen display by lymph node stroma promotes T cell tolerance to intestinal self. Nat. Immunol. 2007; 8:181–190. [PubMed: 17195844]
14. Sanz-Moreno V, et al. Rac activation and inactivation control plasticity of tumor cell movement. Cell. 2008; 135:510–523. [PubMed: 18984162]
15. Wolfenson H, Bershadsky A, Henis YI, Geiger B. Actomyosin-generated tension controls the molecular kinetics of focal adhesions. Journal of cell science. 2011; 124:1425–1432. [PubMed: 21486952]
16. Nimnual AS, Taylor LJ, Bar-Sagi D. Redox-dependent downregulation of Rho by Rac. Nat. Cell Biol. 2003; 5:236–241. [PubMed: 12598902]
17. Krishnan H, et al. Serines in the Intracellular Tail of Podoplanin (PDPN) Regulate Cell Motility. J Biol Chem. 2013; 288:12215–12221. [PubMed: 23530051]
18. Martín-Villar E, et al. Podoplanin associates with CD44 to promote directional cell migration. Mol Biol Cell. 2010; 21:4387–4399. [PubMed: 20962267]
19. Muñoz, BF. Podoplanin association with CD44 and lipid rafts relevance for the regulation of cell motility and epithelial plasticity. 2010.
20. Fernández-Muñoz B, et al. The transmembrane domain of podoplanin is required for its association with lipid rafts and the induction of epithelial-mesenchymal transition. Int. J. Biochem. Cell Biol. 2011; 43:886–896. [PubMed: 21376833]
21. Mourão-Sá D, et al. CLEC-2 signaling via Syk in myeloid cells can regulate inflammatory responses. Eur. J. Immunol. 2011; 41:3040–3053. [PubMed: 21728173]

Europe PMC Funders Author Manuscripts

22. Yang C-Y, et al. Trapping of naive lymphocytes triggers rapid growth and remodeling of the fibroblast network in reactive murine lymph nodes. Proc. Natl. Acad. Sci. U.S.A. 2013; 111:E109–18. [PubMed: 24367096]

23. Tozluoğlu M, et al. Matrix geometry determines optimal cancer cell migration strategy and modulates response to interventions. Nat. Cell Biol. 2013; 15:751–762. [PubMed: 23792690]

24. Chyou S, et al. Coordinated regulation of lymph node vascular-stromal growth first by CD11c+ cells and then by T and B cells. The Journal of Immunology. 2011; 187:5558–5567. [PubMed: 22031764]

25. Mammoto A, Mammoto T, Ingber DE. Mechanosensitive mechanisms in transcriptional regulation. Journal of Cell Science. 2012; 125:3061–3073. [PubMed: 22797927]

26. Calvo F, et al. Mechanotransduction and YAP-dependent matrix remodelling is required for the generation and maintenance of cancer-associated fibroblasts. Nat. Cell Biol. 2013; 15:637–646. [PubMed: 23708000]

27. Fletcher AL, et al. Reproducible isolation of lymph node stromal cells reveals site-dependent differences in fibroblastic reticular cells. Front Immunol. 2011; 2:35. [PubMed: 22566825]

28. Gaggioli C, et al. Fibroblast-led collective invasion of carcinoma cells with differing roles for RhoGTPases in leading and following cells. Nat. Cell Biol. 2007; 9:1392–1400. [PubMed: 18037882]

Europe PMC Funders Author Manuscripts

Europe PMC Funders Author Manuscripts

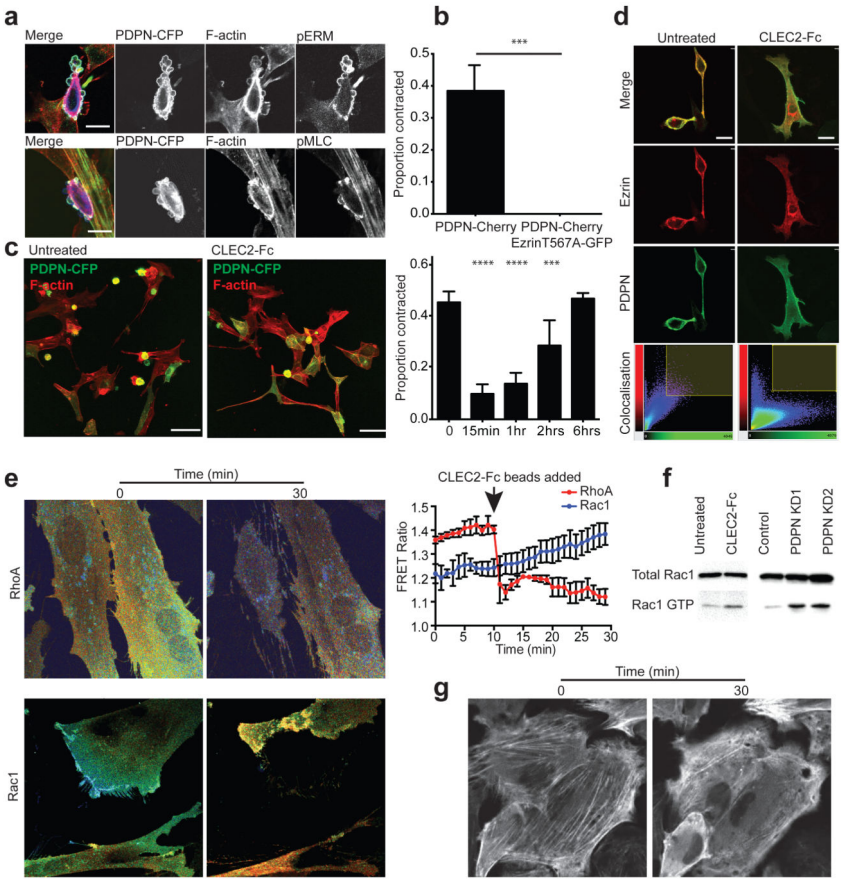

Figure 1. CLEC-2 binding uncouples PDPN from RhoA/C- and actomyosin-driven fibroblast contractility

a) NIH/3T3 expressing PDPN-CFP (blue) or untransfected (control), fixed and stained for pERM (green) or pMLC (S19) (green) and F-actin (red). Scale bar 20 μm. **b)** Frequency of contracting NIH/3T3 expressing PDPN-cherry or PDPN-cherry and Ezrin T567A-GFP. **c)** NIH/3T3 expressing PDPN-CFP (green) stained F-actin (red) treated with 10 μg/ml CLEC-2-Fc (15 min). Scale bar 50 μm. Quantification in the right panel depicts mean ± SD of 3 experiments (>300 cells). Fisher's exact test (****, $p< 0.00005$, ***, $p< 0.0005$). **d)** NIH/3T3 expressing PDPN-CFP and Ezrin-mCherry treated with 10 μg/ml CLEC-2-Fc (15 min). Single optical slice (1 μm), scale bar 20 μm. Pixel colocalisation analysis is shown at bottom. **e)** FRC cell lines expressing RhoA or Rac1 FRET biosensors exposed to CLEC-2-Fc-coated beads. Quantification of FRET ratio is shown on right and depicts mean ± SD of 15 cells from 2 independent experiments. **f) Left:** total and GTP-bound Rac-1 in lysates from FRCs treated with 10 μg/ml CLEC-2-Fc (30 min). **Right:** same analysis in two independent PDPN-knockdown FRC lines (KD1 and KD2) vs. control line. **g)** FRC cell lines expressing GFP-MLC (grayscale) treated with CLEC-2-Fc-coated beads.

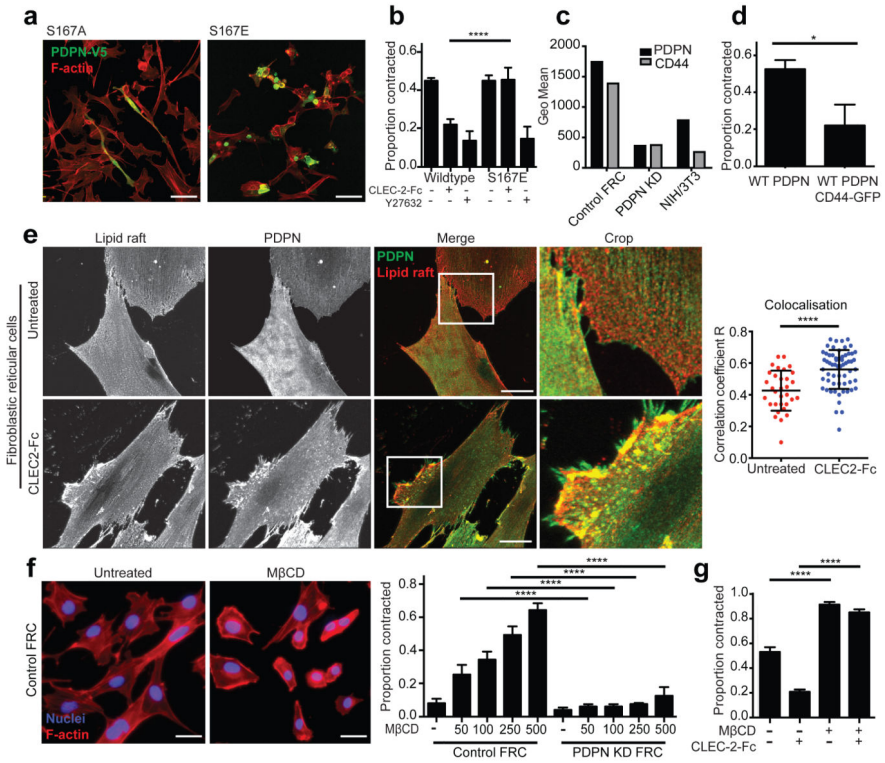

Figure 2. CLEC-2 binding causes redistribution of PDPN within the plasma membrane

a) NIH/3T3 expressing V5 tagged-PDPN mutants (PDPN-V5) stained for V5 (green) and F-actin (red). Scale bar 50 μm. **b)** Contraction score of NIH/3T3 expressing WT or mutant PDPN treated with 10 μM ROCK inhibitor (Y27632) (6 hours) or 10 μg/ml CLEC-2-Fc (30 min). Mean ± SD of 3 independent experiments (>300 cells). Fisher's exact test (****, p<0.00005). **c)** Surface expression of PDPN and CD44 in the indicated cells as analysed by flow cytometry **d)** Contraction score of NIH/3T3 expressing PDPN-V5 ± CD44-GFP. Mean ± SD of 3 experiments (>150 cells). Fisher's exact test (p<0.05). **e)** Confocal slices (0.5 μm) showing surface staining of lipid rafts and PDPN on primary FRCs treated with 10 μg/ml CLEC-2-Fc protein (45 min). Scale bar 50 μm. Colocalisation correlation coefficient R is shown on right; each point represents one cell. Mann Whitney U test (****, p<0.0001). **f) Left:** FRC cell lines treated with 250 μM MβCD (6 hours) stained for F-actin (red) and DNA (blue). Scale bar 50 μm. Right: contraction score in the indicated FRC cell lines treated with MβCD. Mean ± SD of 3 experiments >300 cells. Fisher's exact test (****, p< 0.00005). **g)** Contraction score in PDPN-CFP-expressing NIH/3T3 pretreated with 250 μM MβCD (6 hours) and subsequently treated with 10 μg/ml CLEC-2-Fc (15 min). Mean ± SD of 3 experiments (>300 cells). Fisher's exact test (****, p< 0.00005).

Europe PMC Funders Author Manuscripts

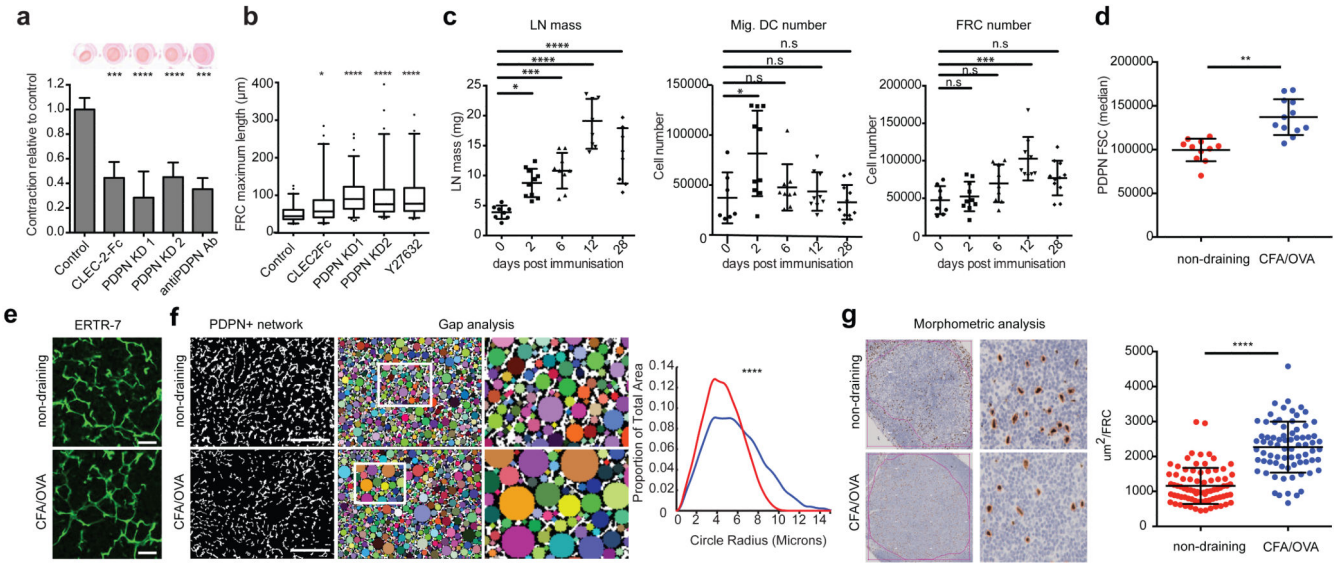

Figure 3. The FRC network stretches to accommodate acute increases in LN cellularity

a) Collagen matrix contraction by FRC cell lines treated with 10 µg/ml CLEC-2-Fc, anti-PDPN antibody or stably depleted of PDPN. Representative image is shown above. Mean ± SD 8 replicates from 2 experiments. 1-way ANOVA, Dunnetts multiple comparisons (***, p<0.0001, ****, p<0.00001) **b)** Maximum 3-dimensional length from cells as in (a) calculated from 100 µm confocal z-stacks. Graphs indicate median, 25th and 75th percentiles (Range 10-90 percentile). 2 independent experiments (>80 cells). 1-way ANOVA, Dunnetts multiple comparisons (*, p<0.05, ****, p<0.00001). **c)** LN mass, number of migratory DCs ($CD45^+$ $CD11c^+$ $MHCII^{hi}$) and number of FRCs ($CD45^-$ $PDPN^+$ $CD31^-$) in LNs draining the site of OVA/CFA immunisation. Each point represents one LN. Mean ± SD 2 experiments with 8-12 mice per timepoint. Day 0 represents non-immunised mice. 1-way ANOVA, Tukey's multiple comparisons (*, p<0.05, **, p>0.001, ***, p>0.0001, ****, p<0.00001). **d)** Forward scatter of FRCs following OVA/CFA immunisation (day 6). Mann Whitney U test (**, p< 0.001). **e)** ER-TR7 staining (green) of the T cell zone of draining or non-draining LNs following OVA/CFA immunisation (day 6). Scale bar 30 µm. **f) Left:** PDPN staining (white) of LN sections as in (e) converted to binary images for gap analysis. Scale bar 100 µm. **Right:** Gaps (coloured circles) within the FRC network. White box = area at higher magnification. Quantification is shown on far right. p = 4.194e-09 (proportion of radii> 15 µm), Fisher's exact test. **g)** Morphometric analysis of GFP^+ nuclei (FRCs) in draining or non-draining LN sections from PDGFRaKI-H2B-GFP mice following CFA/OVA immunisation (day 6) (left). anti-GFP (brown), hematoxylin (blue). Quantification of average area occupied by individual FRCs is shown on right. Data in f and g are from multiple sections from 8 mice in 2 independent experiments. Mann Whitney U test (****, p< 0.00001).

Europe PMC Funders Author Manuscripts

Europe PMC Funders Author Manuscripts

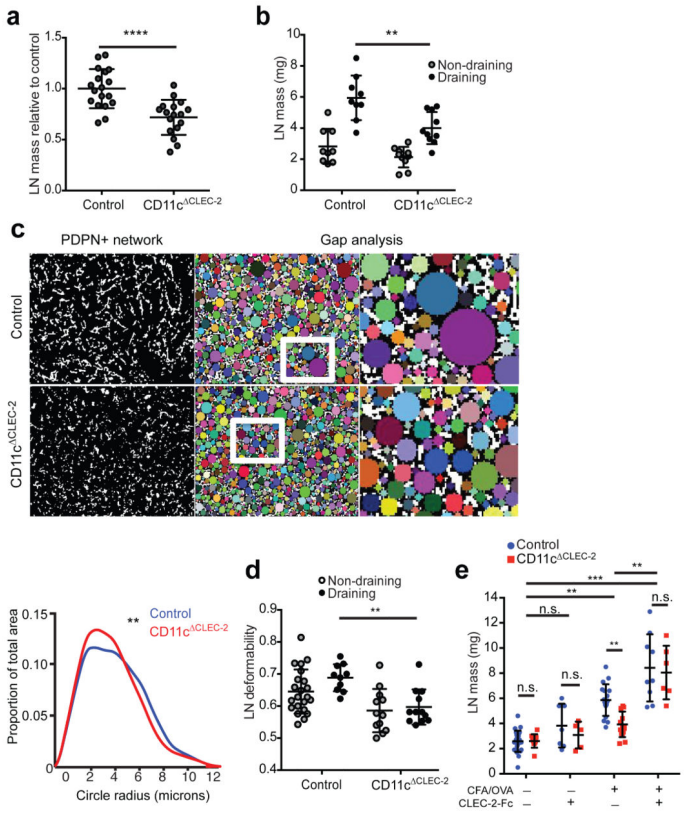

Figure 4. CLEC-2^{+} dendritic cells are required for LN swelling during adaptive immune responses

a) Mass of skin draining LNs from CD11c$^{\Delta CLEC\text{-}2}$ mice and Cre^{neg} littermate controls, >24 weeks old. Data are normalised to average LN mass of Cre^{neg} control. Each data point represents 1 LN. Mann Whitney U test (****, p< 0.00001). **b)** LN mass (mg) of draining and non-draining LNs from 8-12 week old CD11c$^{\Delta CLEC\text{-}2}$ mice and Cre^{neg} littermates (control) immunised with OVA/CFA (day 7). Each point represents a LN. Data from 3 experiments. 2-way ANOVA, Tukey's multiple comparisons (**, p< 0.001). **c)** Gap analysis of draining LNs from immunised control (top) and CD11c$^{\Delta CLEC\text{-}2}$ mice (bottom), quantified on the right. p = 0.0001759 (radii> 8 μm), Fisher's exact test. **d)** LN deformation following compression of whole LNs with 1.4N force. Each point represents one LN. p<0.05, 1-way ANOVA. **e)** LN mass of CD11c$^{\Delta CLEC\text{-}2}$ mice and Cre^{neg} littermates (control) 7 days following CFA/OVA immunisation and treatment with 10 μg CLEC-2-Fc or PBS (days 1 and 3). Each point represents one LN, data from 3 experiments. 2-way ANOVA, Tukey's multiple comparisons test (**, p< 0.001; ***, p< 0.0001; n.s., non-significant).